Influence of the Flow Field on the Flame Propagation in a Hydrogen-Fueled Internal Combustion Engine

Author, co-author list (Do NOT enter this information. It will be pulled from participant tab in MyTechZone)

Affiliation (Do NOT enter this information. It will be pulled from participant tab in MyTechZone)

ABSTRACT

The flame propagation in an optically-accessible hydrogen-fueled internal combustion engine was visualized by high-speed schlieren imaging. Both fully homogeneous and stratified mixtures were evaluated for two intake configurations: low tumble with a tumble ratio of 0.22, corresponding to unmodified intake ports, and high tumble with a tumble ratio of 0.70, resulting from intake modification. To stratify the mixture, the fuel was injected early during the compression stroke from an angled single-hole injector, adding significant momentum to the in-cylinder flow. High-speed schlieren imaging during combustion allowed deducing the apparent flame speed, which was then correlated with in-cylinder pressure measurements on a single-cycle basis.

In a typical cycle, flame shape and degree of convection are heavily affected by the in-cylinder flow. For homogeneous fueling with low tumble, the flame shows little convection and evolves without significant wrinkling with a shape that is quite symmetric in the vertical plane. In contrast, in the other cases, the flame is heavily convected and stretched. Ensemble-averaged results show that for fully homogeneous conditions, the increase in tumble ratio from 0.22 to 0.70 results in increased flame growth and shorter combustion duration. For the stratified mixture, two regimes were observed: During the early part of the combustion, the flame grows faster for high intake-induced tumble, while during middle and late combustion low tumble yields a faster burn rate with an overall shortest combustion. Single-cycle analysis indicates that early flame development dictates the "quality" of a cycle in that the estimated flame speed strongly correlates with the crank angle at which 5% mass fraction of the fuel is burned. Convection is characterized by the displacement of the flame's projected area centroid, revealing that the multi-cycle centroid cloud spreads with time and that the cycles follow different paths according to their flame speed: typically the slow cycles stay near the ignition point and at the top of the centroid cloud. Finally, the ensemble-averaged flame centroid and its apparent speed were estimated. These results show that for the DI cases centroid speeds are relatively high during the start and then slowly decrease as the flame evolves. In contrast, the homogeneous flames show a convective speed that is nearly constant.

INTRODUCTION

Hydrogen-fueled internal combustion engines (H2ICEs) with near-zero emissions levels and efficiencies higher than modern diesel engines are attractive power plants for automotive applications [1-3]. Current research efforts in advanced H2ICEs are devoted to achieving break thermal efficiencies higher than 45% while keeping levels of NOx emissions low [2, 3]. To accomplish this goal, modern H2ICEs use direct injection (DI) fueling strategies [4-7]. In typical DI-H2ICE operation the fuel is injected into the cylinder after IVC. This increases the volumetric efficiency and mitigates knock, pre-ignition and backfire, negative effects associated with hydrogen port-fuel injection [4, 8].

Flame propagation in spark ignited (SI) engines fueled by hydrocarbon fuels is well-studied and the controlling factors are mostly understood [9-11]. Alefeiris [11], for example, reports that for stratified lean operation the flame development is affected by the fuel distribution and flow field around the spark plug, residual gas, spark energy, and the heat loses to the electrodes. Among these factors, the community has devoted special attention to the effects of fuel distribution and flow field on combustion stability, especially when

the engine operates near the lean limit [12-20]. Lean operation, either in premixed or DI engines, can have significant benefits in efficiency and emissions [9, 21]. However, close to the lean limit, combustion becomes "unstable", that is, there is large cycle-to-cycle variation (CCV) in performance-determining parameters like burn duration. To achieve stable operation near the lean limit, charge stratification, by gasoline direct injection (GDI) and enhancement of the in-cylinder turbulence have been used. In the case of charge stratification, mixture preparation enters as an additional process complicating combustion control [16].

In hydrocarbon-fueled SI engines combustion is typically divided in four stages: ignition and flame initiation, initial flame kernel development, fully developed turbulent flame propagation, and flame termination [22]. All stages contribute to the overall combustion process; however it has been shown that the first two stages are the ones that determine the quality[1] of the cycle and have direct influence on the CCV [23]. For example, several studies show that there is a strong correlation between the crank angle corresponding to 5% mass fraction burned (CA Xb =5%) and the IMEP [10, 24]. The CA Xb =5% choice is subjective: smaller values of Xb are difficult to measure due to the finite accuracy of in-cylinder pressure measurements. Nevertheless, CA Xb =5% represents a time span corresponding to the initial flame-kernel development. The limitations of pressure measurements in determining how early the Xb defines the quality of a cycle have been overcome by imaging the temporal evolution of the flame kernel. Imaging allows resolving very small Xb and has proven to be very useful in characterizing the combustion process and its associated temporal and spatial CCVs [10, 14, 18, 20, 24-27].

Concerning the influence of in-cylinder flow, it is well established that in gasoline (SI) engines the intake-induced in-cylinder flow has significant effect on engine performance and emissions [16, 28]. "Tumble", a coherent rotation of the in-cylinder charge around an axis perpendicular to the cylinder axis, is believed to influence combustion characteristics by breaking up into small-scale turbulence late during the compression stroke [28-30]. This increases turbulence intensity and thereby the turbulent flame speed, which promotes faster combustion, extends the lean limit of stable engine operation, lowers knock propensity, and reduces cyclic variability. However, high convective velocity also increases heat transfer to the relatively cold walls of the combustion chamber [9]. In hydrogen engines at low loads, due to the relatively long combustion duration in ultra-lean operation, this tumble break-down may be particularly important for combustion and hence engine performance.

Recent studies in our engine show that in DI-H2ICEs the intake-induced flow field has a significant influence on the final fuel distribution, even though the injection event completely alters the pre-injection flow [31-33]. Due to the relevance of these results for the present study, an abbreviated sequence of flow-field measurements during the compression stroke is shown in Figure 1. Two cases were compared: The unmodified intake-port configuration ("low tumble"), and a tumble-enhanced modified version ("high tumble"). Without injection, at bottom dead center (BDC[2]) for the low tumble case the flow consists of two weak, counter-rotating vortices. The in-plane tumble ratio (TR) is 0.22. During the compression stroke, the flow develops an upward-welling pattern as the tumble ratio gradually approaches zero near top dead center (TDC). Conversely, for the high-tumble configuration, a single, well-defined vortex describes the flow field throughout most of the compression stroke. At BDC the TR is 0.70, decreasing to 0.25 at -30°CA. With fuel injection, the fuel jet, issued from an angled single-hole nozzle just after intake-valve closure, impinges on the liner and forms a wall jet. Entraining the cylinder charge during the compression stroke, the wall jet imparts a tumble-like global rotation onto the charge. Due to the injector targeting, injection-induced convection and intake-induced tumble flow counter-act, hence the high tumble case is in general retarded in the development of its circular convection pattern. The final mixture distribution, investigated separately [31], is significantly different between the two cases.

Due to the unique properties of the hydrogen fuel [8], the existing knowledge about flame propagation for hydrocarbon fuels cannot be simply extrapolated unchecked to hydrogen engines. Consequently, since flame propagation is at the heart of efficiency and emissions, we need experimental data on flame propagation in H2ICEs. Visualization of flames in hydrogen-air mixtures in constant volume vessels is reported in the literature for atmospheric and higher pressures [34-36]. These studies have focused on the characterization of laminar burning velocities with the main goal of finding correlations that could be used in combustion submodels

---

[1] Here, the quality of a cycle is measured by its IMEP, i.e. a good cycle has high IMPE while a not too good cycle has a relatively low IMEP.

[2] The crank-angle convention used here assigns 0 °CA to TDC, i.e., crank angles throughout the compression stroke are negative.

of multidimensional simulations of H2ICEs. To complement such studies under stationary conditions, present work investigates flame propagation in an operating engine with a realistic fuel distribution and flow field. Also, while previous studies [6, 31-33] concerned the mixture-preparation phase only, the present work investigates the influence of the in-cylinder flow field on combustion as well. To this end, flame propagation was visualized by high-speed schlieren imaging, complemented by classic fast cylinder-pressure measurements. "Movies" of flame propagation, from ignition to 50°CA after ignition, were recorded for homogeneous and stratified mixtures (from fuel DI) for the same two intake configurations that were investigated in the flow measurements shown above. By correlating these image series with the pressure measurements, the effects of enhanced tumble were evaluated. The present measurements are also very suitable to validate future numerical simulations of the combustion process in DI-H2ICEs and will be added to the Engine Combustion Network [37], an internet data-base for validation of engine simulations.

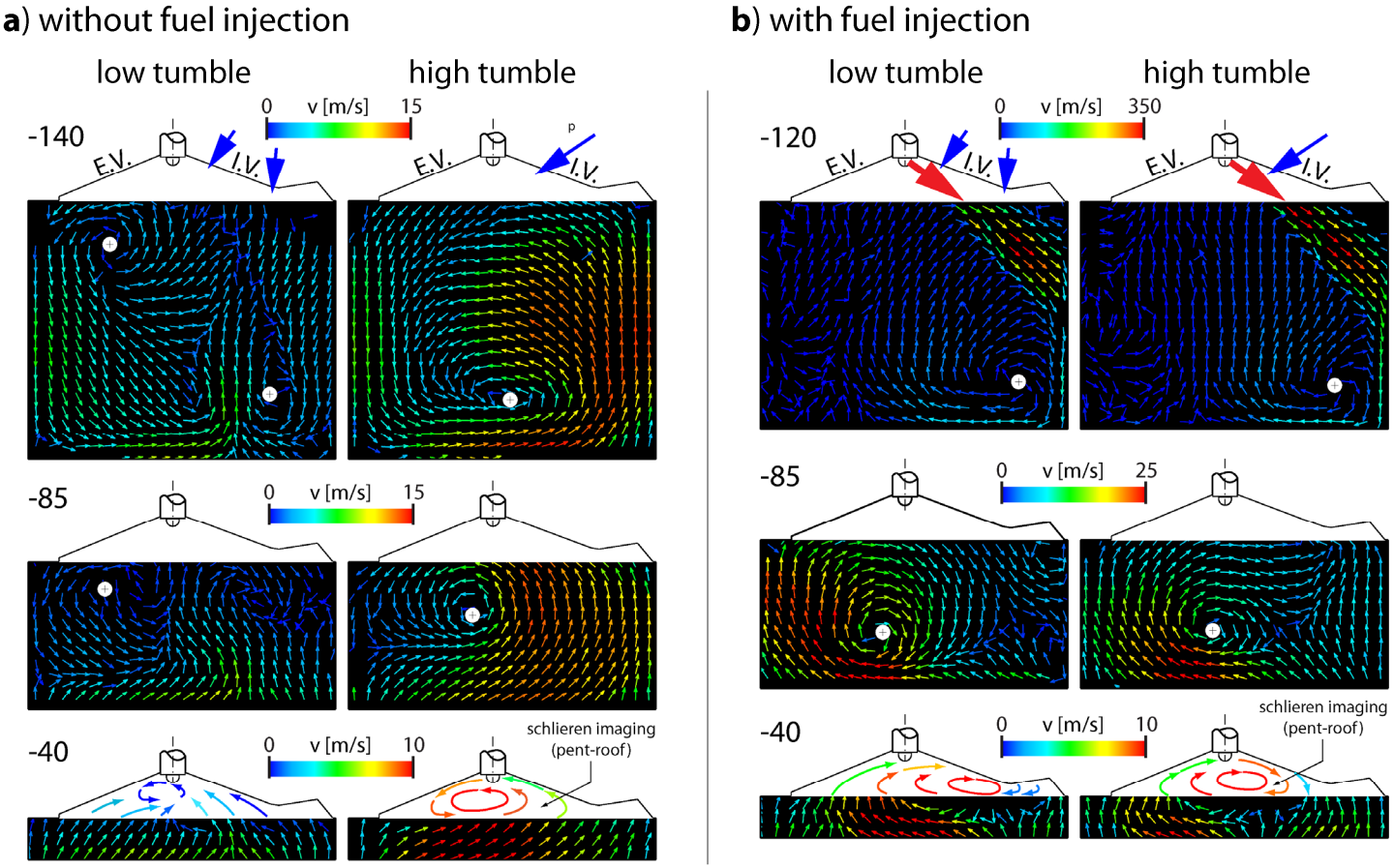

Figure 1 - In-cylinder flow in the central symmetry plane during compression, measured by PIV in previous work [33]. Blue arrows indicate the main direction of intake-flow momentum for the two different intake configurations. (a) Without fuel injection, (b) with fuel injection just after IVC, indicated by the red arrows. Note that the velocity color-scale is different for each vector plot. At -40°CA the likely flow pattern in the pent roof, which was not part of the measurement domain, is shown schematically.

EXPERIMENT

OPTICAL ENGINE AND HYDROGEN INJECTOR

Experiments were performed using a passenger-car sized optically accessible single-cylinder engine adapted to operate with hydrogen. Schematics of the relevant optical and mechanical components are shown in Figure 2. The engine uses a four-valve four-stroke single-cylinder GM research head with a pent-roof combustion chamber. The piston is flat-topped. The engine head has not been modified for hydrogen fueling other than the injector. The intake system consists of two intake ports, one for each valve, both straight and parallel to each other forming an angle of 40° with respect to the fire deck (horizontal). Some engine parameters are given in

Table 1. Hydrogen was supplied at 100 bar directly into the combustion chamber via a solenoid injector from Westport Inc. As shown in Figure 2a, the injector nozzle has a single hole with a diameter of 1.46 mm at a 50° angle with respect to the injector axis. Figure 2b shows the injector location, centrally located between the four valves, and the nozzle direction, aiming towards the intake between the two valves and downward. Hence the jet was aligned with the mirror-symmetry plane of the combustion chamber.

Table 1 – Engine Specifications

Bore	92 mm
Stroke	85 mm
Displacement	565 cm^3
Compression ratio	11
Speed	1500 rpm
Intake pressure / Temperature	1 bar / 36°C
Intake valve timing	open: 346°CA / close: -140°CA
Exhaust valve timing	open: 130°CA / close: -356°CA
Injection timing	start: -137°CA / end: -119.5°CA

VISUALIZATION OF FLAME PROPAGATION

Flame propagation was visualized by schlieren imaging with a high-speed camera, illustrated schematically in Figure 2d. Since schlieren techniques have been used for many years to visualize density gradients in transparent media [38], only a brief description of the description of the optical system will be given. The arrangement was that of "focused shadowgraphy" in "Z" layout [38] with the engine's pent-roof as the imaged object. Light from a green, pulsed, high-power light-emitting diode (LED) was focused through an aperture with 0.7 mm diameter and collimated by a parabolic mirror with a focal length of 900 mm. Figure 2c shows the region of the combustion chamber that was accessible via flat, fused-silica windows on each end of the pent-roof. After passing through the engine's pent-roof, the collimated beam was focused by another, identical parabolic mirror through a round aperture with 1.7 mm diameter, which acted as a schlieren stop. A camera lens with focal length f = 100 mm projected the resulting schlieren images onto the detector of a high-speed complementary metal-oxide-semiconductor (CMOS) camera (Phantom v7.1). Single-cycle sequences of images were acquired with a temporal frame spacing of 0.5°CA (= 55 μs) and an effective exposure time of 5.5 μs, given by the LED's pulse width. The visual contrast between burnt and unburnt regions in the schlieren images was enhanced by temporal differentiation, *i.e.*, by subtracting the previous frame from each frame [39]. For each condition, simultaneous schlieren sequences and pressure traces of 140 cycles were recorded.

In the current engine configuration the hydrogen injector replaces the spark plug when mounted centrally in the combustion chamber. Therefore, in fired operation ignition was achieved by creating a laser-induced plasma at the approximate location of the spark gap (if the spark plug were mounted), as shown in Figure 2c. Omitting the spark plug removes the associated aerodynamic obstruction of the in-cylinder flow such that the movement of the nascent flame kernel can be observed better, but slight differences from the early flame development with a proper spark plug may result. A detailed investigation of laser ignition in hydrogen-fueled engines is outside of the scope of the current effort. Instead, given the optical access of the engine, laser ignition simply provided a convenient means of firing the engine to observe the effects of charge motion on flame propagation. Laser ignition has previously been used in engines running on gaseous fuels, for example [40, 41], and in liquid-fueled engines [42]. Outside of engines, many studies of laser ignition of flammable gas mixtures have been performed. Most pertinently, in lean hydrogen-air mixtures, the laser-induced plasma and flame-kernel formation has been imaged in a constant-volume vessel [43]. In the current experiments, a localized plasma was created by focusing two consecutive pulses from a dual-head Nd:YAG laser at 1064 nm with a spherical lens with f = 150 mm. The pulse separation was 500 μs (= 9°CA) ; each pulse had an energy of 40 mJ. The timing of the first laser pulse is taken to be ignition timing. Flame-front visualization was performed for maximum brake-torque (MBT) spark timing.

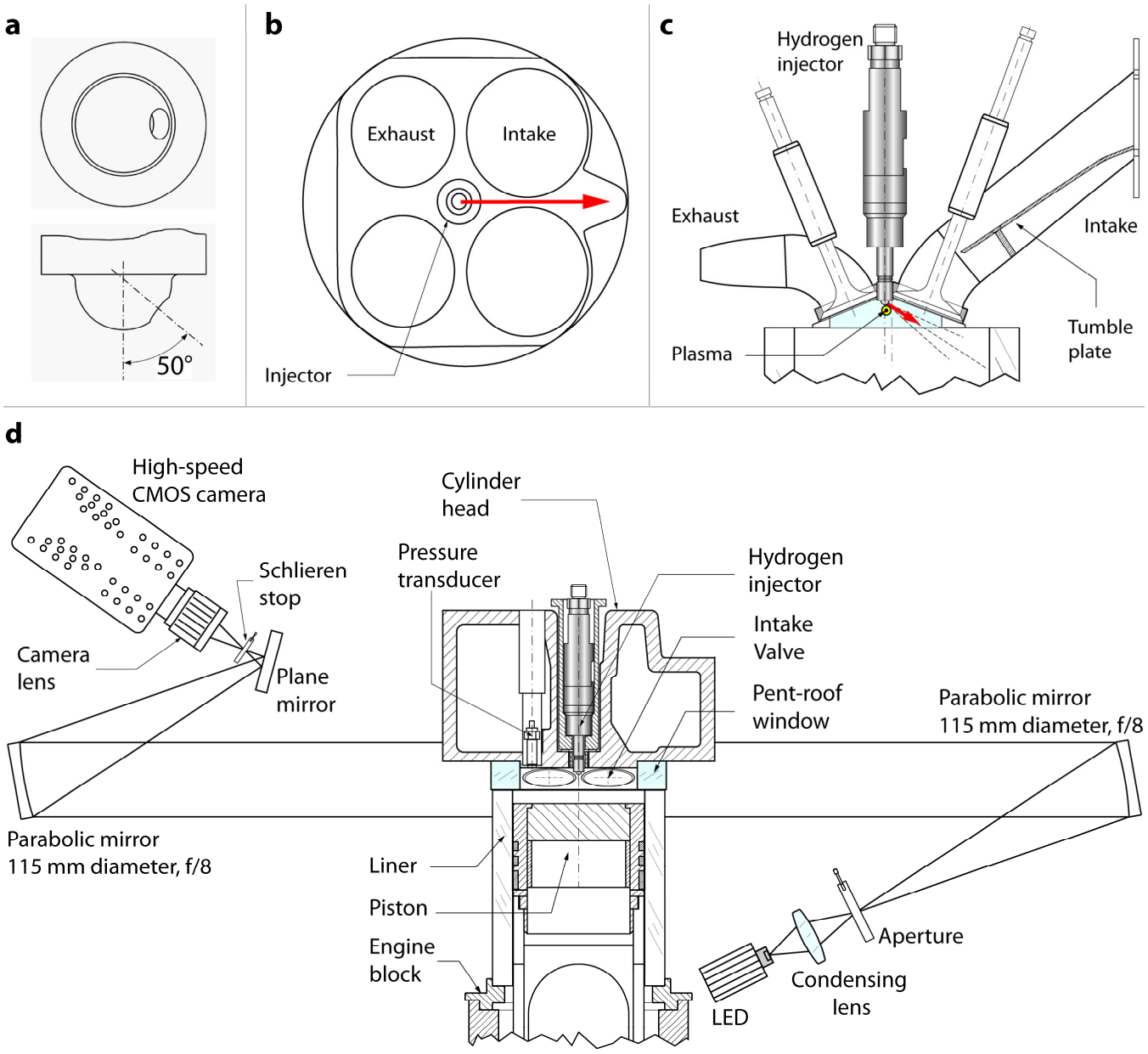

Figure 2 - Schematics of engine hardware. (a) Geometry of the single-hole injector nozzle, (b) location and targeting of injector with respect to the combustion chamber, (c) pent-roof window, and position of laser-plasma ignition, (d) upper engine and schlieren-imaging system.

EXPERIMENTAL CONDITIONS

Two different modes of engine operation are considered in this study: Fired with a fully homogeneous fuel/air mixture, and fired with DI. In both cases, the engine was fired every fifth cycle while the speed was kept constant at 1500 rpm. For DI operation, the pressure in the surge tank upstream of the intake runner was kept at 1 bar and typical intake temperatures, just upstream of the engine head, were around 36°C. In premixed operation, the intake pressure was raised to 1.1 bar to achieve the same time-averaged fuel and air flows as with DI.

With DI, to obtain a global equivalence ratio of 0.25 ($\lambda = 4.0$) or a hydrogen mole-fraction of 0.095, the hydrogen fuel was injected for 17.5°CA at 100 bar. In fired operation at typical efficiencies, this fuel concentration represents a low-load condition with about 2.5 - 2.7 bar indicated mean effective pressure (IMEP). As in previous studies [31-33], the fuel injection started shortly after intake-

valve closure to yield the maximum time span to interact with the intake-induced flow. With the injection command issued at -140°CA, flow from the nozzle started at -137°CA and ended at -119.5°CA. For premixed operation, fuel was supplied sufficiently far upstream that complete mixing of fuel and air could take place.

As in the previous study summarized by Figure 1, two different intake configurations were used: the unmodified intake and a modified version yielding an approximately four times higher tumble ratio. There are several ways to increase the tumble ratio in an engine [14, 28, 44]. Here, we inserted tongue-like plates into the intake ports, gradually reducing the cross-section of each port to its upper half, thereby directing the intake flow more along the pent-roof than would be the case without modifications. The engine head with tumble plates is shown in Figure 2c. In the following, when comparing operation with the unmodified head to that with tumble plates inserted, the former will be addressed as "low tumble" and the latter as "high tumble" operation. For each intake-flow condition, flame propagation was visualized for premixed air/fuel supply and with DI, with the former supply option presumably yielding in-cylinder flow identical to that without fueling, as investigated as a baseline in previous work.

RESULTS AND DISCUSSION

In this section, a morphological comparison of single-cycle sequences of schlieren images for the different configurations will be described. Then, the flame area evolution and its variability as a function of time after ignition are discussed. The section concludes with an extensive study of the flame-propagation speed and flame location which are correlated with engine performance on a single-cycle basis.

VISUALIZATION OF THE EARLY FLAME DEVELOPMENT AND ENSEMBLE-AVERAGED HEAT RELEASE

Figure 3 shows typical[3] single-cycle sequences of schlieren images, labeled by degrees crank angle after ignition timing (°CA aIT), with the engine operating at maximum brake-torque spark timing (see Table 2). At ignition, 0°CA aIT, for all configurations a well-defined round plasma of similar size can be observed. This plasma then develops into a flame kernel, which by 2.5°CA aIT already shows strong influence of the in-cylinder flow. Wrinkled borders, typical of turbulent premixed combustion, become visible in all flames. As time progresses, the effects of the flow becomes more obvious as it drives flame evolution. For the homogeneous mixture with low tumble, the flame evolves radially outwards from the plasma and remains quite symmetric with respect to the pent-roof, resembling a growth similar to what is observed in pressurized vessel experiments [35, 36]. Previous velocity measurements [33], summarized in Figure 1, showed that near TDC the flow field does not have a single vortical structure; instead, a weak upwelling flow develops during compression, presumably supported by piston motion. This is consistent with the lack of convection and distortion in the flame shape for this case.

With high tumble, just after ignition the large-scale flow structures convect the evolving flame kernel toward the exhaust valves. Initially, the kernel is small and it is only wrinkled by the smallest flow-scales. However, as the flame grows, the kernel becomes progressively wrinkled by larger flow scales until its size is sufficient to experience the whole spectrum of turbulent length scales. In Figure 3, this takes place around 5°CA aIT; beyond that, the flow also starts to stretch the flame in two directions: along the exhaust side of the pent-roof and towards the center of the combustion chamber. The flow measurements in Figure 1 [33] suggest that the intake-induced tumble vortex survives until the end of compression. Based on these two observations (i.e., flow and flame), vortex break-down [14, 28] has not taken place or is at least not completely. Figure 3a shows qualitatively that for high tumble flame propagation is faster. This faster propagation appears to be enhanced by convection and stretching effects, not only by small-scale turbulence from tumble break-down. However, Figure 3a represents only one single cycle, and indeed there are sometimes cycles in which the flame evolves as in the low tumble case, indicating that a strong vortical structure is not always present.

---

[3] The issue of what is "typical" is central to cycle-resolved measurements of engine combustion. Statistical analysis, some of which is performed in subsequent sections, is necessary to define "typical" behavior. Here we simply mean that the image sequences were chosen such that their morphological features, as described in the text, can be recognized in the majority of sequences from the same conditions. Exceptions are explicitly mentioned.

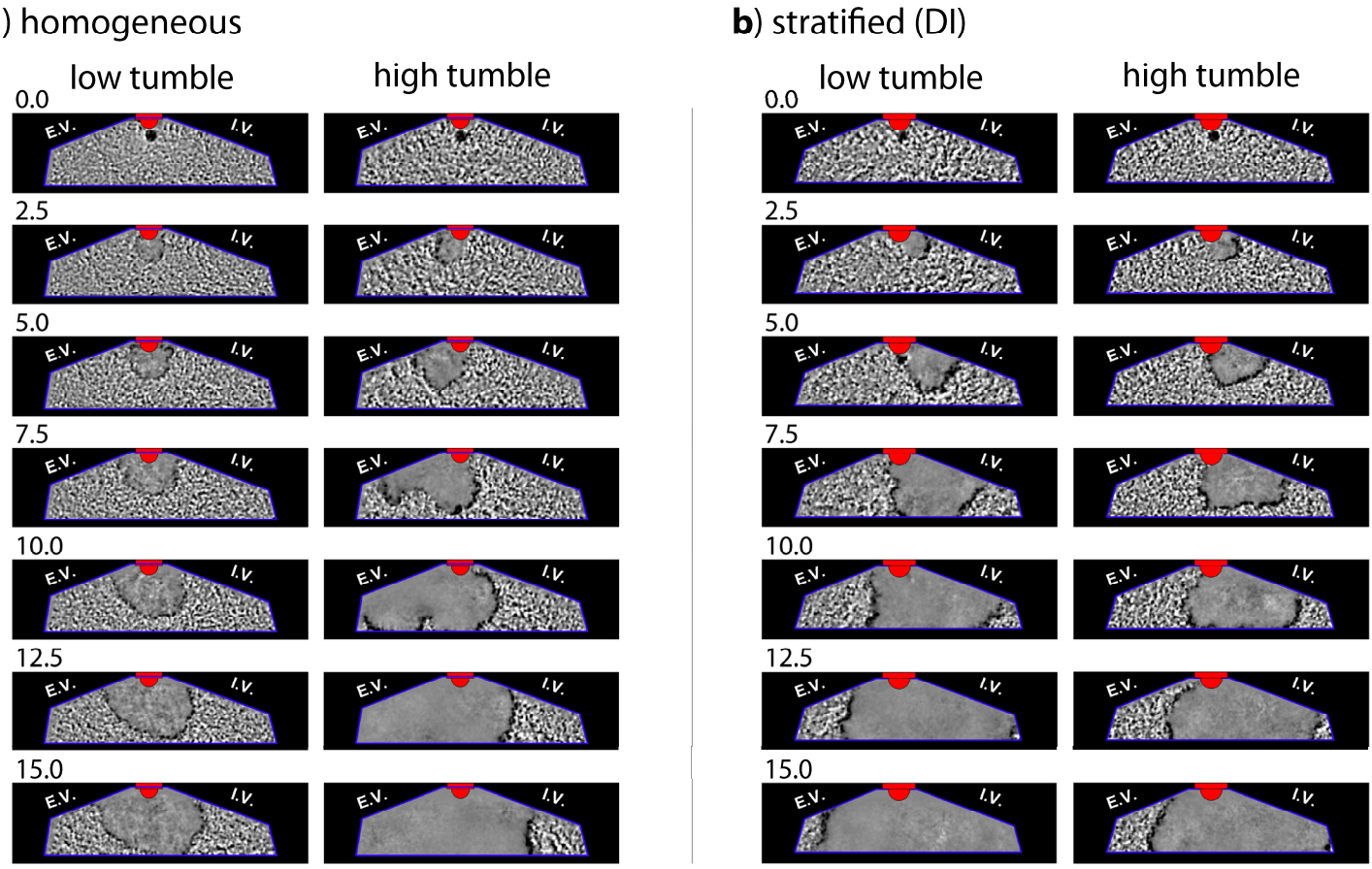

Figure 3 - Flame propagation in (a) homogenous and (b) stratified (DI) hydrogen/air mixtures for low and high tumble. Typical single-cycle sequences of schlieren images are shown, labeled by degrees crank angle after ignition. Approximate locations of intake valves (IV) and exhaust valves (EV), and injector (red) with respect to the pent-roof windows are also shown.

Before we turn our attention to the DI cases, we compare the schlieren-visualized combustion process to the ensemble-averaged apparent heat release, derived from the in-cylinder pressure data using a single-zone heat release analysis [9], shown in Figure 4a for homogenous fueling. Table 2 also lists performance measures derived from pressure traces. Consistent with the morphology of the typical cycles shown in Figure 3a, high tumble yields much faster heat release during the entire combustion, with an overall reduction of the 0-90% burn duration from 95°CA to 77°CA. Engine thermodynamics have a notorious lack of repeatability in optical engines; nevertheless, the measured improvement in indicated thermal efficiency (ITE) and coefficient of variation (COV) in IMEP is qualitatively consistent with the shorter burn duration. Note how small the COV of IMEP is despite ultra-lean, homogeneous operation, which is due to the unique physio-chemical properties of hydrogen as a fuel [8].

With DI, in Figure 3b the effect of flow field on flame kernel development is also clearly visible. Similarly to the homogeneous high tumble case, initial solid-body flame convection is followed by a strong stretch of the flame. Since the injection event causes inversion of the tumble direction [33], the flames are convected and stretched clockwise. Qualitatively, both flames have the same features and propagate at similar speed. However, Figure 4b shows a faster heat-release rate for high tumble during the initial part of combustion (until about 20°CA aIT). Although visualization of the flame front during the intermediate and late combustion was not possible, the heat release analysis in Figure 4b indicates that contrary to the first part of the combustion, after 20°CA aIT the low-tumble case releases heat faster than its high-tumble counterpart. As a result, the total combustion duration is shorter for this case. It is well known [25, 45, 46] that early flame-kernel development is affected by the equivalence-ratio around the kernel. Therefore, a plausible explanation for the trends observed above could be that while the presence of a richer fuel cloud dominates early combustion, a stronger more turbulent in-cylinder flow overcomes the fuel effect during middle and late stages. In general, the differences between the two tumble configurations are small for DI, and the particular injection geometry appears to create a “super

tumble" case in both flow and flame propagation. Consistent with this broad generalization, with DI the burn duration is shorter, while both ITE and COV of IMEP are improved with respect to homogeneous operation with high intake-induced tumble.

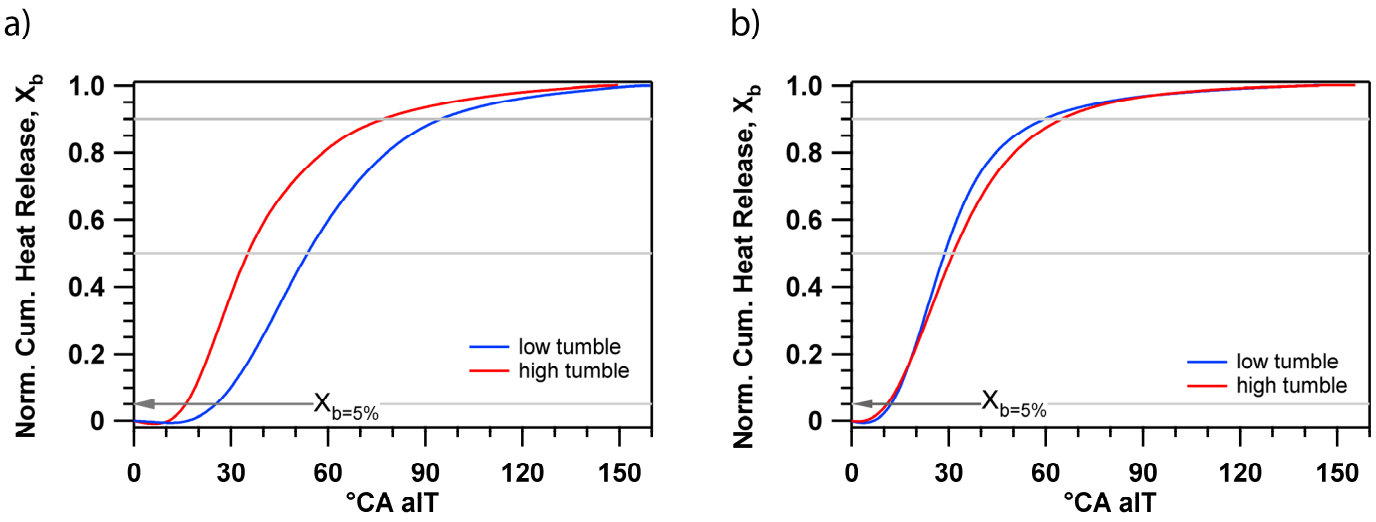

Figure 4 - Normalized cumulative heat release, Xb , for (a) homogeneous and (b) stratified (DI) hydrogen/air mixtures for low and high tumble. Also indicated is the crank-angle at which the mass fraction burned reaches 5%.

Table 2 – Spark Timing and Performance Measures

	Hom. low tumble	Hom. high tumble	DI low tumble	DI high tumble
MBT spark timing [°CA]	-30	-20	-20	-26
Indicated thermal efficiency [%]	32.5	33.1	35.4	34.2
COV of IMEP [%]	3.7	2.9	1.4	2.0
0-90% Burn duration [°CA]	95	77	60	65

CYCLIC VARIABILITY ANALYSIS

Qualitative observations of typical cycles and ensemble-averaged results are useful for an initial understanding of the general features of each case. However, cycle-resolved measurements allow further insight into the stochastic nature of in-cylinder phenomena via quantitative statistical analysis.

DEVELOPMENT OF THE FLAME-KERNEL AREA

For single-cycle analysis, the flame area was calculated from binarization of the schlieren images as shown in Figure 5a-b. This methodology allowed tracking the flame growth as a function of time in a single-cycle basis. Due to the cyclic variation of the in-cylinder flow, the flame area scatters significantly from cycle to cycle. To visualize this variability, in Figure 6 and Figure 7 the average flame area is plotted with error bars representing ± one standard deviation, both for homogeneous and for DI mixtures, respectively. Figure 6 shows that for the homogeneous case, the variability for high tumble is significantly larger than for low tumble. This trend is quite interesting, since according to Table 2 one should expect less variability for the high tumble case. Nevertheless, on average, high tumble results in a faster flame growth, which is consistent with the heat release analysis in Figure 4a. With DI, mixture stratification and the strong injection-induced flow clearly increase the flame growth rate (Figure 7) for

both tumble conditions. Although the high-tumble flame has a higher growth rate, which is consistent with the average heat release of Figure 4b, the variability is approximately of the same magnitude for both tumble cases and considerably greater than in the homogeneous cases (Figure 6). If we again interpret the current form of DI to create a "super tumble", it appears that an increase in tumble results in an increase in the variability of the projected flame area. This trend is in contradiction with the findings reported by Arcoumanis et. al. [14] for an SI engine fueled with gasoline and compressed natural gas (CNG), where the authors observed a decrease in the area variability as the tumble ratio was increased. The argument put forth in that work is that this behavior is due to the tumble-vortex breakdown, which results in enhanced turbulence but a weaker mean flow.

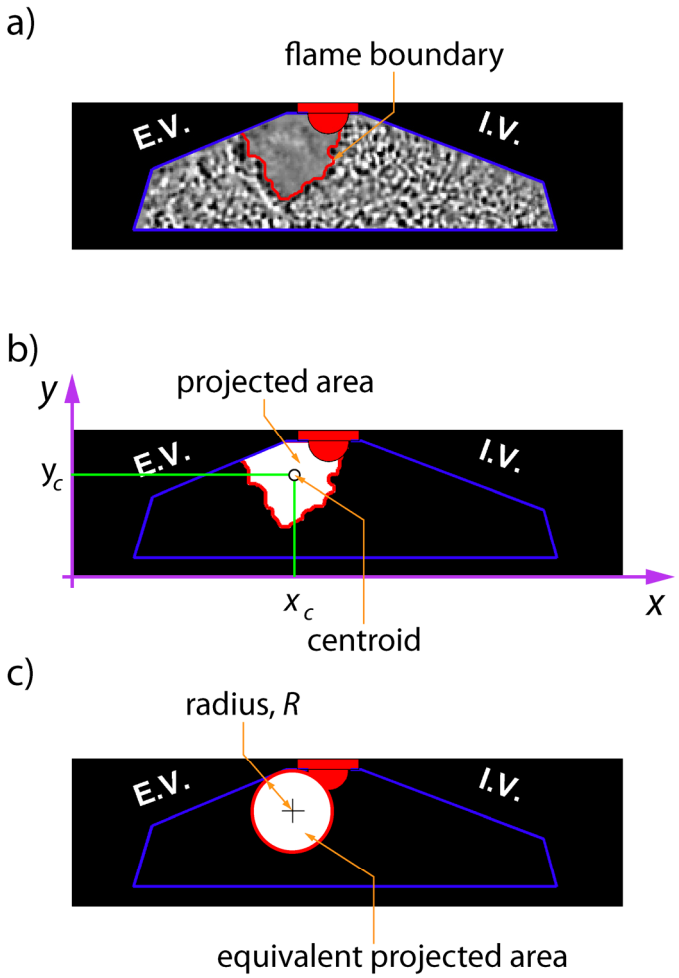

Figure 5 - Binarization process of the schlieren images. (a) Single-shot at a give °CA aIT showing the flame boundary, (b) projected area of the flame and its centroid, and (c) equivalent projected circular area to estimate the flame speed.

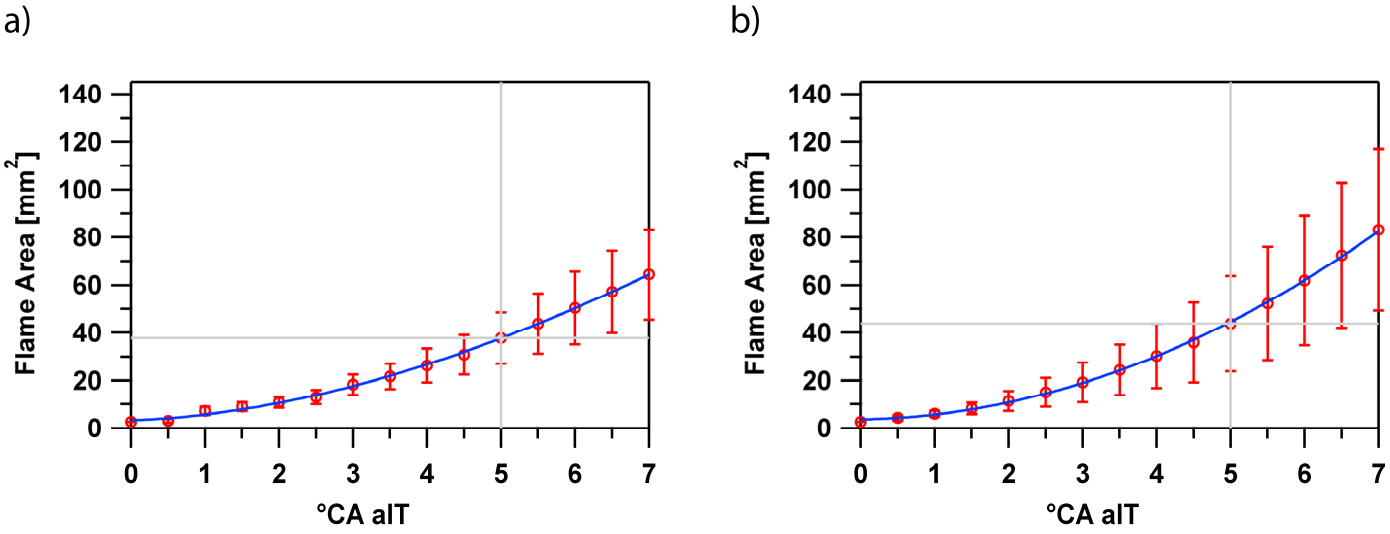

Figure 6 – Evolution of the flame area with homogeneous hydrogen/air mixture for (a) low tumble and (b) high tumble. The vertical bars represent cyclic variation by the standard deviation.

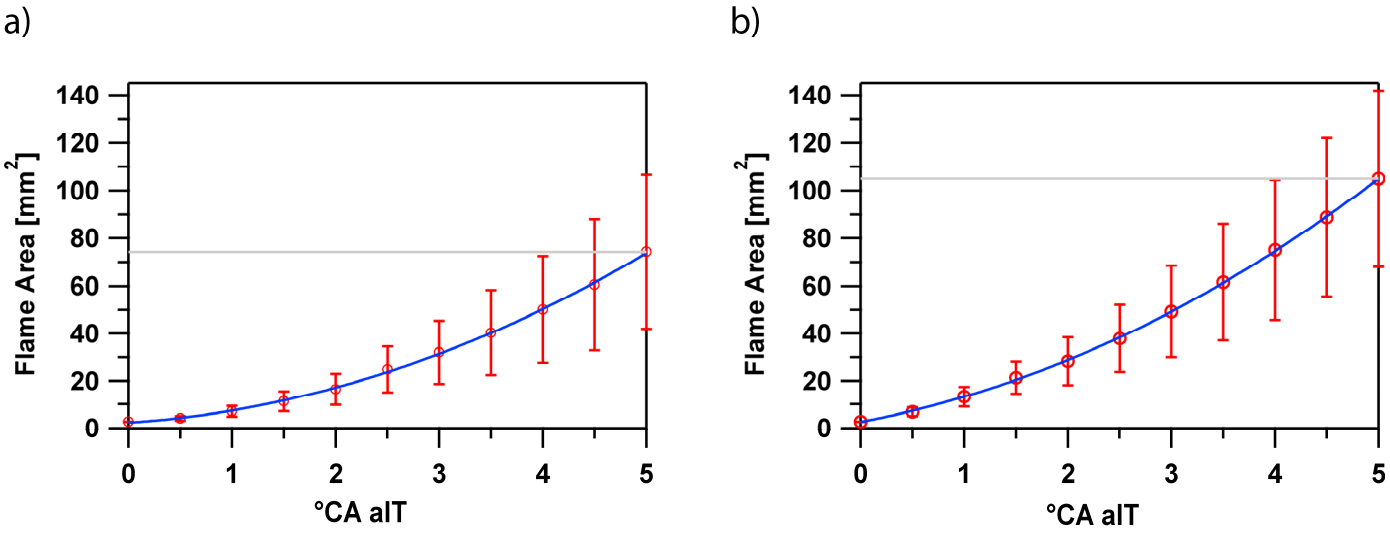

Figure 7 - Evolution of the flame area with stratified (DI) hydrogen/air mixture for (a) low tumble and (b) high tumble. The vertical bars represent cyclic variation by the standard deviation..

To further investigate the role of the flow field on the flame evolution, conditional averaging was performed by dividing the cycles in four groups (0-25%, 25-50%, 50-75%, and 75-100%) according to their combustion phasing [10, 47]. The combustion phasing investigated was the crank angle at which the 5% of the mass fraction is burned, CA Xb =5%, and the assignment into groups was made based on where an individual cycle fell in the total range $(CA\ Xb = 5\%)_{max}$ - $(CA\ Xb = 5\%)_{min}$. Thus, the 0-25% group represents the average of the fastest cycles and those in the 75-100% group are the average of the slowest ones. Figure 8 shows the results for the homogeneous mixture. The unconditional average has also been included to give an indication of how the different groups rank with respect to it. While for low tumble the slow and fast cycles are evenly distributed around the unconditional average, i.e. the average is in between the 25-50% and the 50-75% groups, Figure 8b shows that for high tumble, the 0-25% group is the only one faster than the average; with the remaining groups lying below it. A similar behavior is observed for the DI cases in Figure 9, where the 0-25% groups are the only ones that show a relatively higher growth rate than the average. For low tumble the 25-50% percent group is almost coincident with the average. It appears that with a strong in-cylinder flow, independently of the fueling strategy, the 0-25% group is the only one that is faster than the average.

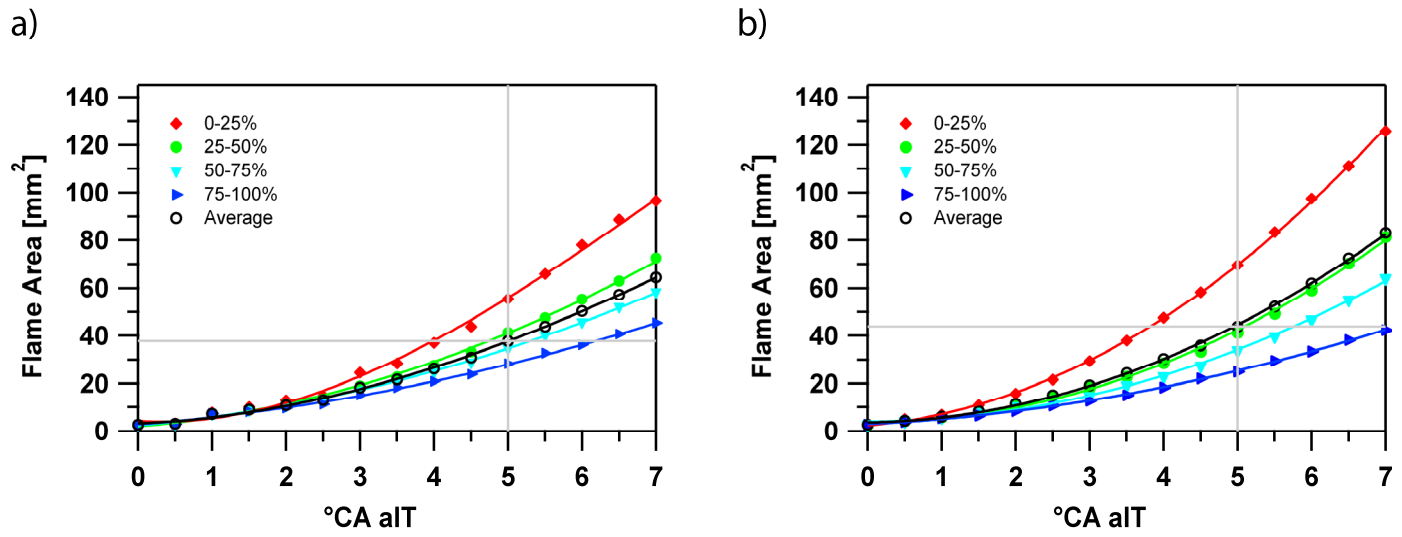

Figure 8 - Conditional average of the flame area with homogeneous hydrogen/air mixture for (a) low tumble and (b) high tumble.

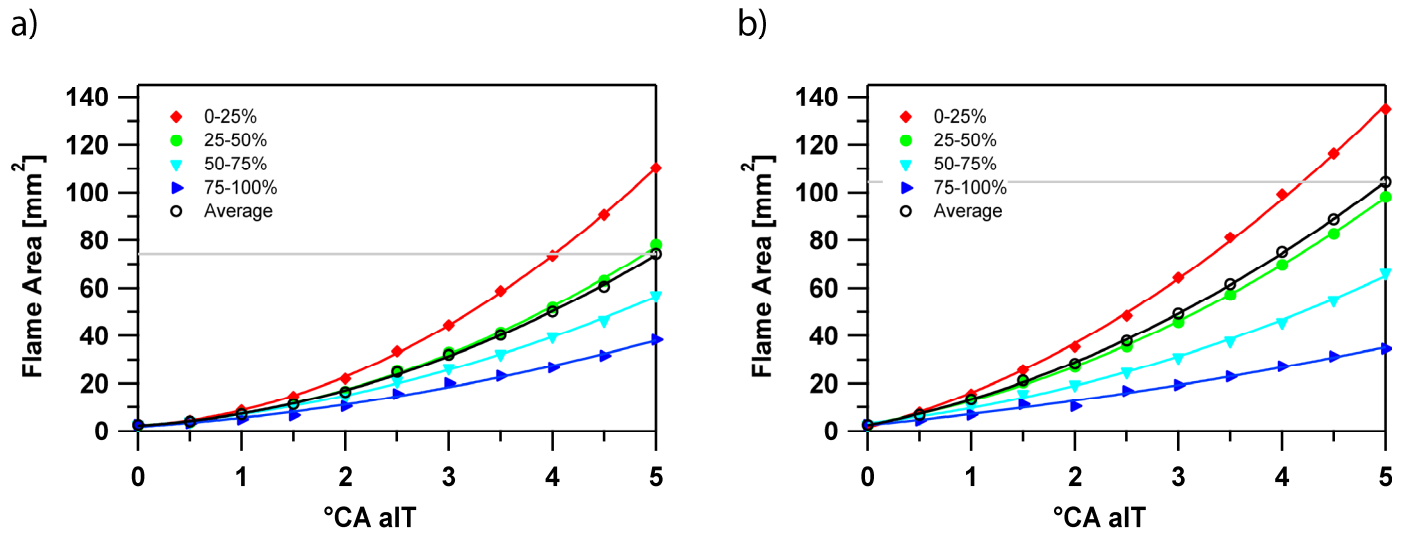

Figure 9 - Conditional average of the flame area with stratified (DI) hydrogen/air mixture for (a) low tumble and (b) high tumble.

FLAME-PROPAGATION SPEED

The flame speed can provide further insight into how the flame evolves on a single-cycle basis. Therefore, from the already-known flame area, the respective equivalent radius R was calculated, which was then used to estimate the flame propagation speed dR/dt (Figure 5c) in every time interval between images from the high-speed camera [24]. It was found that the flames radius increased linearly with time, which indicated that the flame was growing at approximately constant speed. Therefore the flame speed averaged over the first 5°CA aIT was considered to be representative of early flame-kernel development. Figure 10 shows a scatter plot of the crank angle at which the 5% of the mass fraction is burned, CA Xb =5%, versus flame propagation speed. It can be seen that, independently of the fueling strategy and flow field configuration, the flame propagation speed and CA Xb =5% are strongly correlated, demonstrating that the early flame development is an important factor in determining the subsequent timing of CA Xb =5%.

For the homogeneous mixture, the correlations for low and high tumble have different slopes such that in the low tumble case CA Xb =5% is more sensitive to the flame speed. Also, in this case the velocities are scatted in a narrower band, from 2.5 to 6.5 m/s as opposed to 2.5 to 8.5 m/s for high tumble. The former observation has its explanation in the difference in MBT spark timing

between low and high tumble: -30°CA for low tumble versus -20°CA for high tumble. Late spark timing means higher in-cylinder pressure and density, and consequently for the same flame-propagation speed at a given time a greater mass of fuel has been burned. The wider spread in flame speed is consistent with the significantly greater variability of the velocities that was seen in PIV measurements throughout the compression stroke [33] and with the variability in flame area shown in Figure 6.

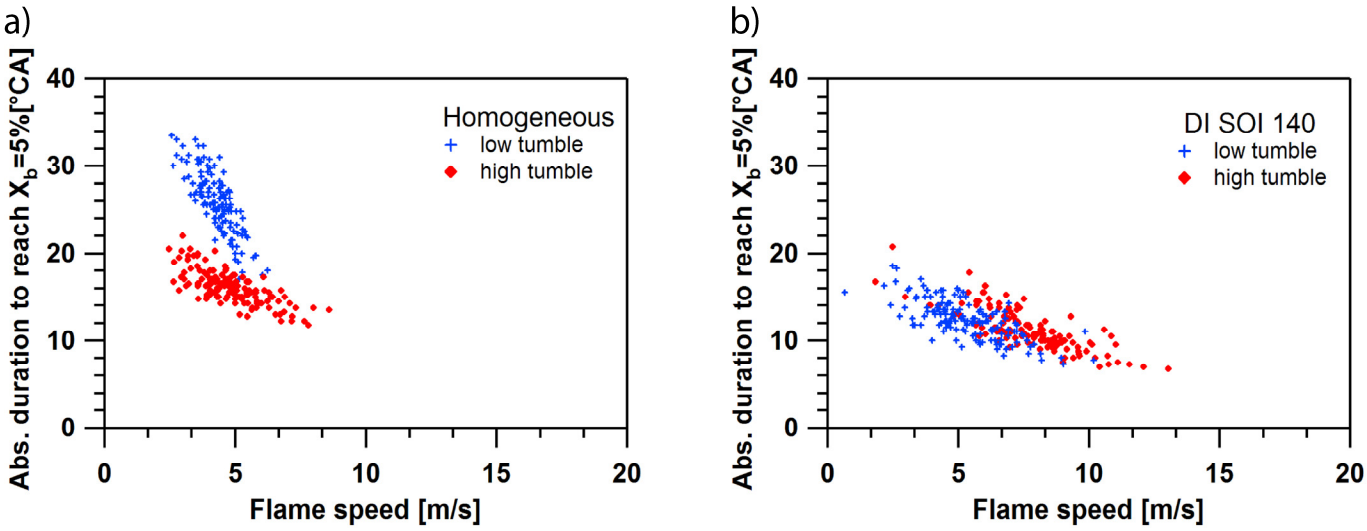

Figure 10 - Relationship between flame propagation speed and the CA to reach a mass fraction burned of 5%, CA Xb =5%, for (a) homogeneous and (b) stratified (DI) hydrogen/air mixtures for low and high tumble.

With DI, the correlation between CA Xb =5% and flame speed is very similar for both intake-flow conditions. Again, the smaller flame velocity for low tumble may also be an artifact of the difference in MBT spark timing. Nevertheless, the point clouds nearly overlap, with high tumble yielding slightly more spread towards higher flame speeds, which coincidently is consistent with the initially faster burn of that case. The reverse difference for the mid and late combustion in Figure 4b cannot be explained with the single-cycle analysis of Figure 10b. Both DI cases have significantly wider spread in flame speed, which again is consistent with increased velocity variability with DI [33] and with the variability in flame area shown in Figure 7.

FLAME CONVECTION

In this section, again following the analysis by Aleiferis et al. and Arcoumanis et al [10, 14, 24], we quantify the convective effect of the flow field on flame displacement. To this end, the location of the flame centroid was determined at every crank angle up to just before, on average, the flame reaches the lower border of the imaged area. For homogeneous operation with low and high tumble this was the case at about 10 and 7°CA aIT respectively, while for all other cases at about 5°CA aIT. Furthermore, to explore if fast cycles follow a different trajectory than slow ones, the centroid location was color-coded by its flame speed.

Figure 11a shows the evolution of the centroid location with respect to the point of ignition and the pent-roof walls for the homogeneous mixture with low tumble. It can be seen that as early as 1 °CA aIT the fast cycles show a preferential displacement towards the bottom edge of the window, while the slowest cycles stay near the ignition point. As combustion progresses, this preferential displacement continues and at the same time the centroids gradually scatter. In agreement with the flow-field measurements [33], the centroids are only convected slightly, remaining close to the ignition point. At 10°CA aIT, when on average the edge of the flame has reached the lower edge of the window, the color coding indicates that the slow cycles still stay around the ignition point. To see if these cycles show some particular features, single-cycle sequences of schlieren images for two representative cycles, slow and fast, are shown in Figure 12a. Morphologically, the slow cycle shows an evolution that is quite symmetric in shape with a flame front that does not wrinkle strongly. The fast cycle, on the other hand, shows a less symmetric shape and has significant wrinkling. These differences could be attributed to the variability in the flow field from cycle to cycle, i.e. for a slow cycle the flow field does not contain the right scales to distort the flame, while for the faster cycles there are flow structures that are strong enough to cause significant flame front wrinkling, increasing turbulent flame speed.

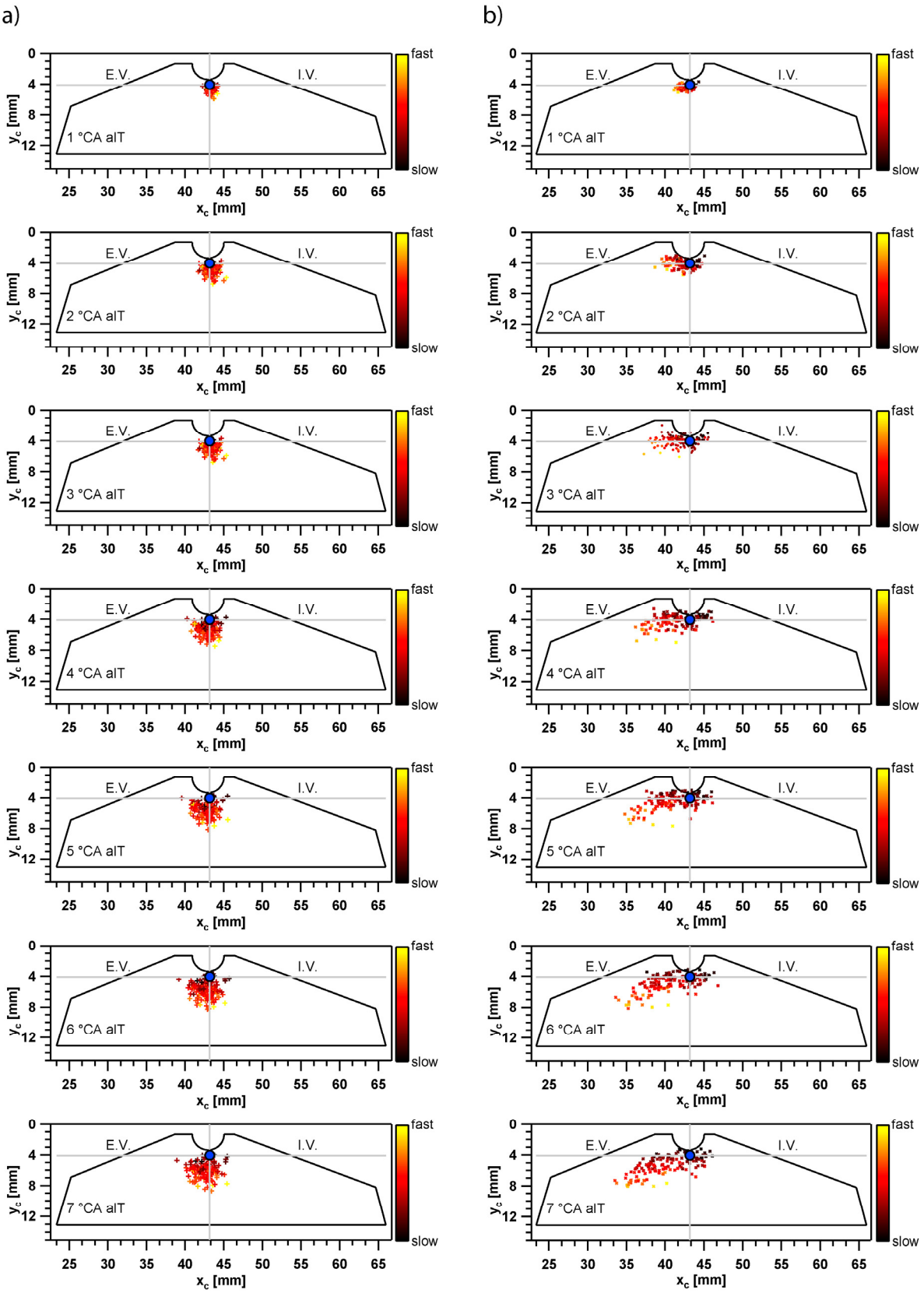

Figure 11 - Location of flame centroids for the homogeneous hydrogen/air mixture with (a) low tumble and (b) high tumble. Blue dots indicate the approximate location of the plasma. The pent-roof window geometry including the injector location is shown schematically.

For high tumble with homogeneous mixture, Figure 11b shows that the convective effect of the intake-induced flow field is present since the very early flame kernel development, when in the majority of cycles the flame is convected toward the exhaust side. However, there are a number of cycles in which the flame remains close to the ignition point, and in some cycles it even moves in the opposite direction (to the right of the ignition point). This supports our initial speculation that the tumble vortex is present in most, but not all cycles. Similar to the low tumble case, the scattering of the centroids cloud increases with time, but at a faster rate and preferentially in the horizontal direction. This trend is consistent with the higher variability of the area growth observed for the high tumble case in Figure 6. Regarding the classification of the cycles as a function of their flame speed, Figure 11b shows that for this condition there is also a clear indication that the slow cycles stay near the ignition point, while the fast cycles are convected by the flow. The fact that the slow cycles stay near the ignition point also indicates that they are subject to a flow field with similar features that the one found in a typical cycle under low tumble conditions. Corresponding slow and fast single-cycle sequences of images shown in Figure 12b support this fact, in that the slow cycle evolves in a manner similar to a typical low-tumble cycle and the fast cycle's flame is convected more and also somewhat more wrinkled. Again, this shows that in a slow cycle the flow field is quiescent and that there is not a tumble vortex.

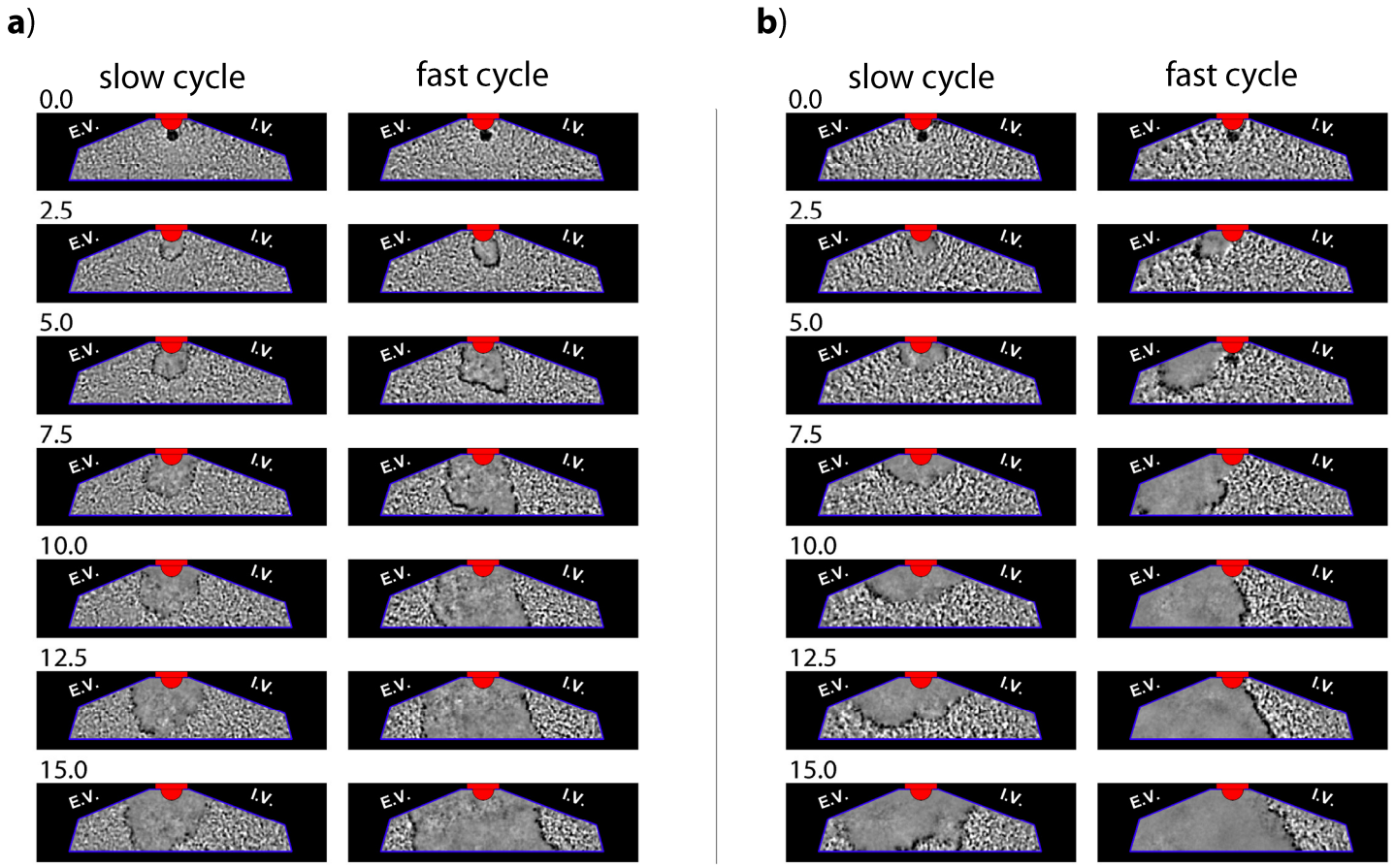

Figure 12 - Flame propagation in an homogenous hydrogen/air mixture with (a) low tumble and (b) high tumble. Typical slow and fast single-cycle sequences of schlieren images are shown, labeled by degrees crank angle after ignition. Approximate locations of intake valves (IV) and exhaust valves (EV), and injector (red) with respect to the pent-roof windows are also shown.

Figure 13a shows the centroid movement for the DI cases. Here, for low tumble, it appears from Figure 13a that the injection-induced flow field persists, displacing the flame kernel in almost all cases. As in the homogeneous mixture cases, the centroid cloud also spreads with time, although at a lower rate than for the high-tumble case, which indicates that the flow field is more stable. At 5°CA aIT, the classification of the cycles by their flame speed shows a clear vertical stratification, with the slowest cycles at the top and the fastest cycles at the bottom. Nevertheless, Figure 14a shows that in both cases there is the signature of a well-defined tumble vortex. What is quite interesting in Figure 13a is to see that the cycles that convect to the left or stay near the ignition point are relatively fast cycles, which is different from what was observed for the homogeneous cases in Figure 11.

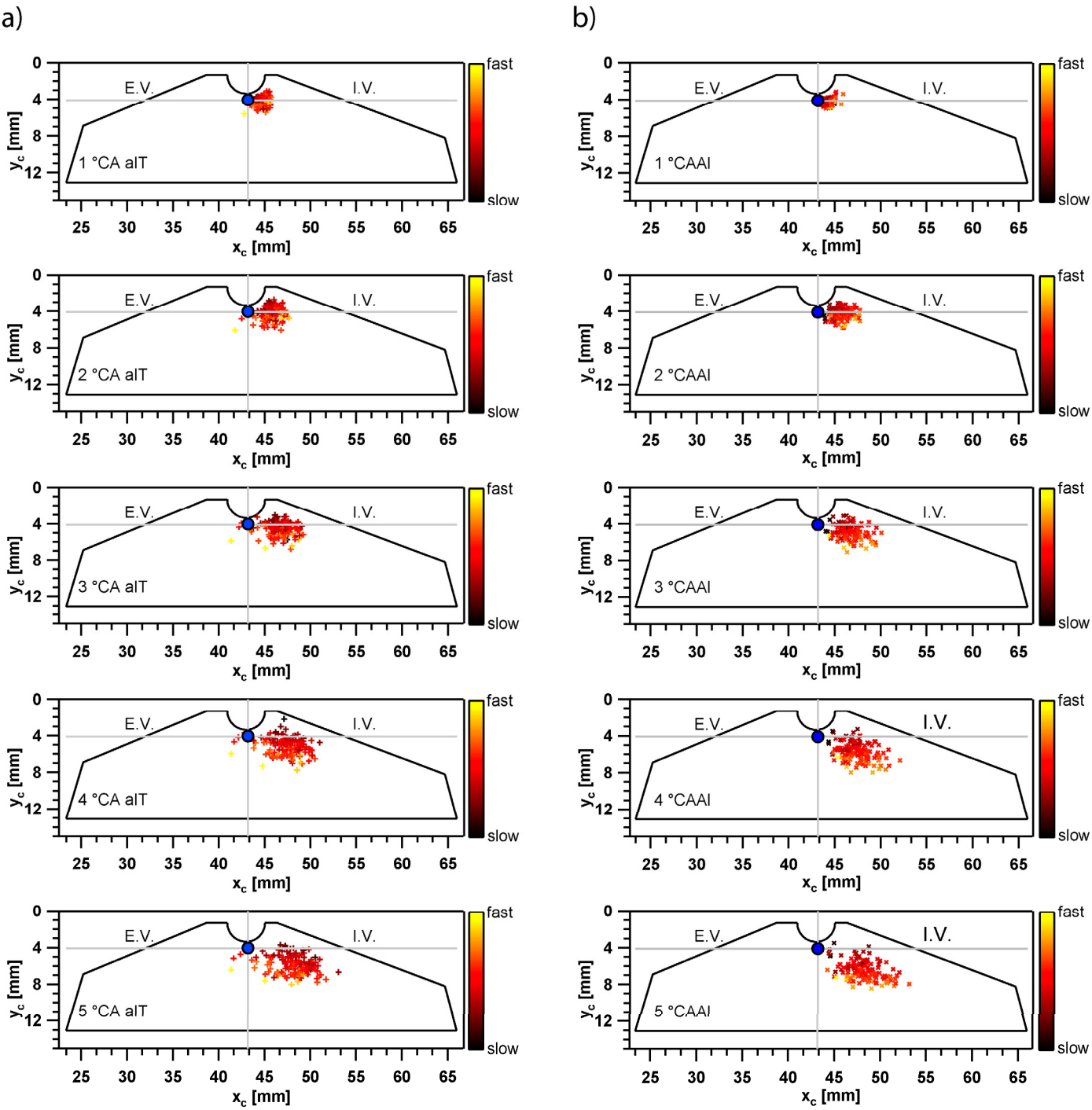

Figure 13.- Location of flame centroids for the stratified (DI) hydrogen/air mixture with (a) low tumble and (b) high tumble. Blue dots indicate the approximate location of the plasma. The pent-roof window geometry including the injector location is also shown schematically.

The flame convection for DI with high tumble, shown in Figure 13b, has features similar to the flame convection observed for the low-tumble case. However, for high tumble in all cycles the flame is convected away from the ignition point, which could indicate that the tumble vortex is more consistent for this configuration. The spatial distribution of the centroids according to their flame speed is also similar to the low-tumble case, with the slowest cycles at the top. The morphology, as shown in Figure 14b, suggests that the difference between slow and fast cycles is also driven by the same mechanism as for the low tumble case (Figure 14a). Unlike the low

tumble case, the cycles with a flame staying near the ignition point are relatively slow, but the flame propagates asymmetrically with respect to the pent-roof. However, for a more definitive statement better statistics would be necessary.

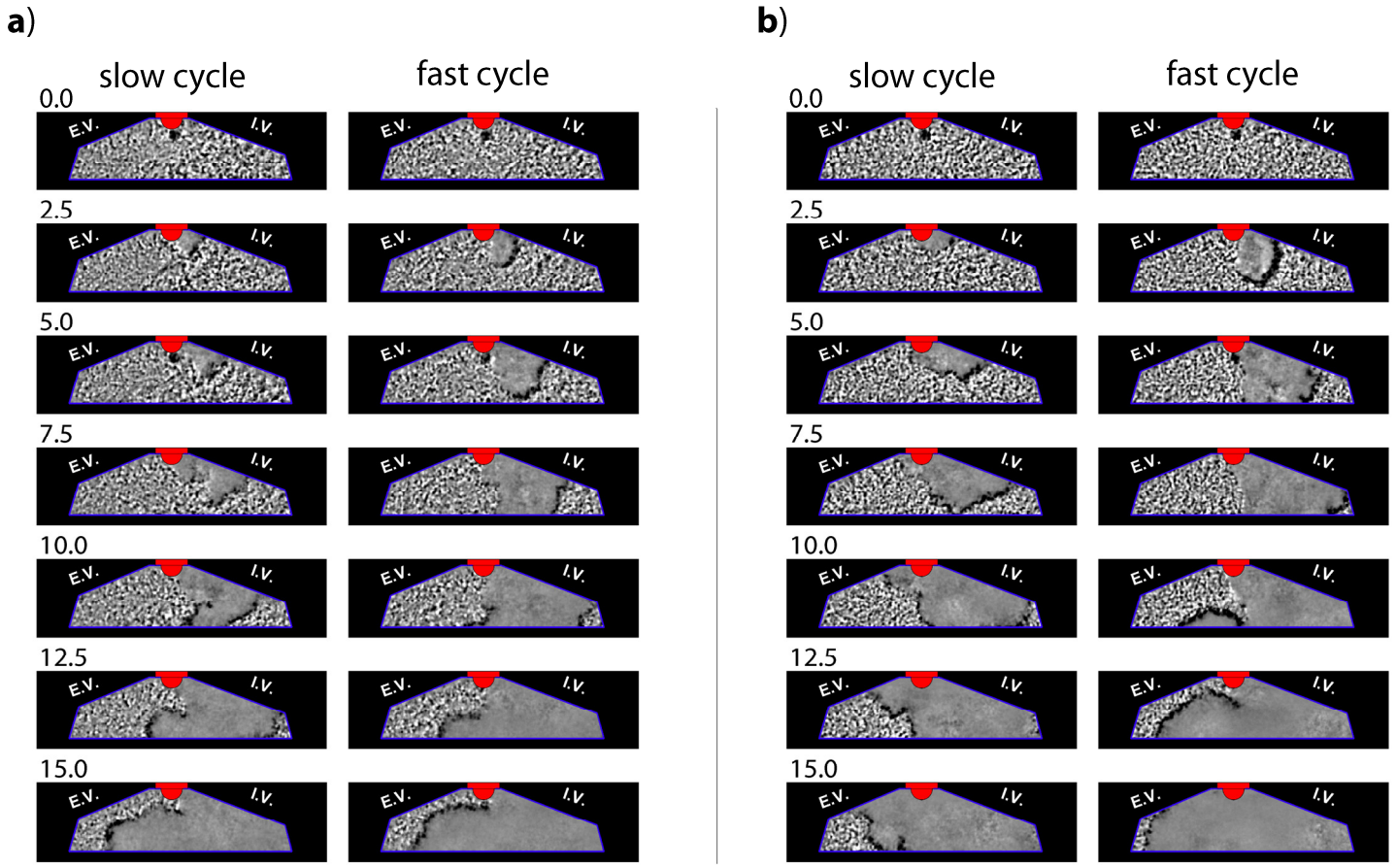

Figure 14 - Flame propagation in a stratified (DI) hydrogen/air mixture with (a) low tumble and (b) high tumble. Typical slow and fast single-cycle sequences of schlieren images are shown, labeled by degrees crank angle after ignition. Approximate locations of intake valves (IV) and exhaust valves (EV), and injector (red) with respect to the pent-roof windows are also shown.

From the description of the flame convection for all the cases, there are two interesting observations to highlight. First, the homogenous high tumble case indicates that although in average the flow field indicates the presence of a strong tumble vortex (Figure 1), there are some cycles when this vortex it is not present, and that these cycles behave in a way similar to a representative cycle in the low-tumble configuration. The second observation is that, at least from the sequences for low and fast cycles, the flames appear to be under the effects of a well defined vortex which does not seem to break down into small scale turbulence as suggested in the literature [14, 28, 29]. For a more detailed analysis and to gain more fundamental insight about the vortex breakdown, flow measurements in the pent-roof itself would be helpful, and such experiments are planned in the near future.

Finally, to consolidate the understanding of flame convection gained so far, the ensemble-average trajectory of the flame centroids is shown in Figure 15. We see that for the homogeneous mixture with low tumble on average the flames move in an almost linear trajectory as they slowly convect downwards and to the left. This is in agreement with the slight asymmetry in the flow field shown in Figure 1 for this condition. For the other cases, the centroid follows a trajectory that somewhat resembles an inverted parabola, which is likely related to the large-scale structure of the tumble vortex. It is also interesting to see that the trajectories for the DI cases have a similar curvature and almost follow the same path. The homogeneous mixture with high tumble, on the other hand, shows a path with a curvature that it is significantly different than of the DI cases. From the trajectories shown in Figure 15 it is also possible to estimate the velocity of the centroid. The results are shown in Figure 16. It is clear that the flame-centroid velocity is much higher for the DI cases. The homogeneous cases have a velocity history that does not significantly change with time, however for the DI cases the velocity is initially high and then gradually decreases. Estimating the velocity from the average flame-centroid trajectory is quite

susceptible to small errors in determining the exact location of the centroid. Nevertheless, these results provide an insight about the magnitude of the speeds at which the flame moves in the combustion chamber, which can be related to the tumble strength.

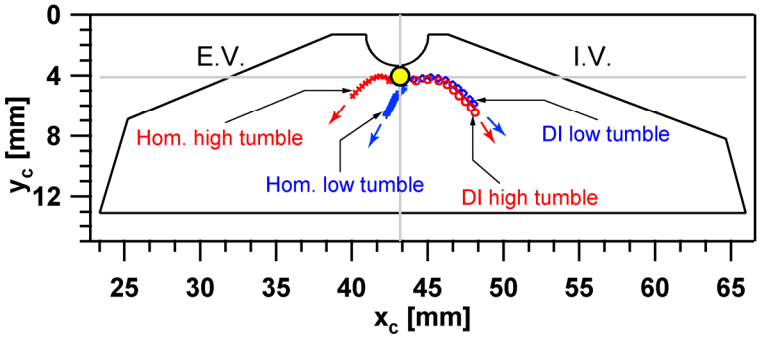

Figure 15 – Ensemble-average trajectory of the flame centroid for the homogeneous and stratified (DI) hydrogen/air mixtures. Approximate locations of intake valves (IV) and exhaust valves (EV), and injector (red) with respect to the pent-roof windows are also shown.

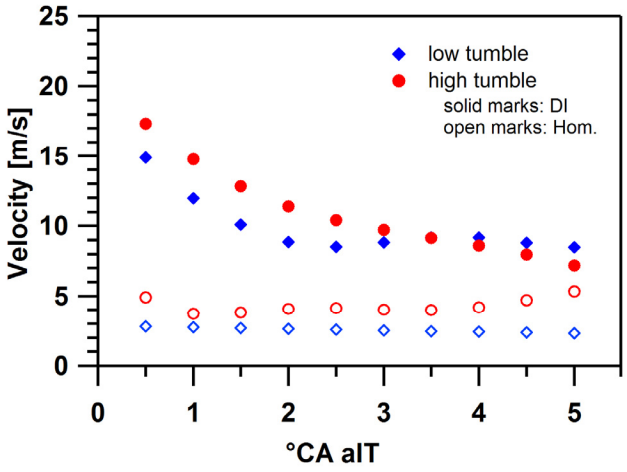

Figure 16 – Flame centroid velocity as a function of the °CA after ignition timing for both homogeneous and stratified (DI) hydrogen/air mixtures for low and high tumble.

CONCLUSIONS

Visualization of flame propagation by high-speed schlieren imaging and simultaneous classic pressure measurements were performed in an optically-accessible hydrogen-fueled internal combustion engine. Both homogeneous and stratified mixtures for low and high intake-induced tumble were investigated. These measurements were intended to complement previous [31-33] measurements of flow field and fuel concentration in the same engine during compression. The main findings of the present study can be summarized as follows:

Morphologically, the flow-field's effect on flame evolution can clearly be seen. For a homogenous mixture with low tumble, the relatively weak in-cylinder flow does not distort and convect the flame significantly, and for nearly all cycles the flame centroid remains near the ignition point. Conversely, the high-tumble case shows effects of convection and stretching for the majority of cycles. However, there are some cycles in which the flame is not convected much, suggesting that the tumble vortex is not present in every cycle. With fuel injection, in nearly all cycles the flame is convected and stretched by the strong injection-induced tumble.

The intake-induced flow has a drastic effect on the development of the combustion event. For the homogeneous mixture, by increasing tumble, the 0-90% burn duration is reduced by approximately 18°CA. A reduction of approximately 30°CA with respect to

homogenous low tumble is achieved by DI with either intake configuration. The COV of IMEP is also improved following the same trend as the burn duration i.e. the highest and lowest COV of IMEP are found for the homogeneous low tumble and for the injection with low tumble, respectively.

Analysis of the evolution of the flame area shows that on average the flame area grows steadily with time and its growth rate is consistent with the reduction in combustion duration observed in the ensemble-averaged apparent heat release. Further single cycle analysis adds evidence that the flame area has significant cycle-to-cycle variability and in all cases this variability grows as the flame evolves. Similarly, it was observed that the area variability, at a given °CA aIT, increases as the growth rate increases, i.e. the variability is the smallest for the homogeneous low tumble case and the highest for the DI high tumble. Additional analysis using conditional averaging based on the Xb = 5% revealed that the quality of a cycle is defined since the very early stages of the flame kernel development, as it is in gasoline engines [24]. Thus, cycles that are fast show a faster growth rate since the early stages. Also, except for the homogeneous low-tumble case, the conditionally averaged groups were not evenly distributed with respect to the average.

The single-cycle analysis also shows that there is a strong correlation between flame-propagation speed and the crank angle at which 5% of the mass fraction is burned (CA Xb =5%) for all conditions examined here. This demonstrates that early flame development is important in determining the subsequent timing of CA Xb =5%. Additionally, it was observed that low tumble with homogeneous mixture has the highest variability of CA Xb =5%, while the injected cases have the lowest, showing a direct correlation with the COV of IMEP.

A detailed study of flame convection provided further insight into how the flames are transported by the in-cylinder flow as they evolve. It was observed that all tested cases featured a progressive scattering of the centroid cloud. However, the degree of this spreading depended of the flow conditions, with the homogeneous high-tumble case showing the highest dispersion. Classification of the cycles according to their flame speed allowed seeing the different paths followed by slow and fast cycles. Typically, the slow cycles stay relatively close to the ignition point and they are found preferentially at the top of the cloud. Nevertheless, there were some outliers, as for example in the DI low tumble case, where some fast cycles stayed around the ignition point and some of them were even convected in the direction opposite to the rotation of the mean tumble vortex. Additionally, the ensemble-averaged trajectory of the flame centroid showed the different paths followed by the flames. For the homogeneous low-tumble case, the flames move in an almost linear path, while for the other cases the flames follow a parabolic trajectory. Finally, an estimation of the velocity at which the average centroid moves along the path indicated that for the homogeneous cases the speed is nearly constant, while for DI the velocity is higher at the start, gradually decreasing as the flame kernel grows.

As a final point, we would like mention again that from the results presented in this paper it is not possible to definitively elucidate if or how much the widely reported tumble breakdown actually does take place. Our results suggest that for the cases studied here such events may not take place or at least not completely. Therefore, to gain additional insight in this respect, velocity measurements in the pent-roof together with a POD analysis are planned in the future. This will also be useful to shed more light on why slow and fast cycles follow the different paths.

ACKNOWLEDGEMENTS

The excellent technical support by G. Hux is greatly appreciated. Financial support for this research was provided by the U.S. Department of Energy, Office of Energy Efficiency and Renewable Energy, program manager Gurpreet Singh. The research was performed at the Combustion Research Facility, Sandia National Laboratories, Livermore, California. Sandia is operated by Sandia Corporation, a Lockheed Martin Company, for the United States Department of Energy's National Nuclear Security Administration under contract DE-AC04-94AL85000.

REFERENCES

1. Edwards, R., Mahieu, V., Griesemann, J.-C., Larivé, J.-F., and Rickeard, D. J., 2004, "Well-to-Wheels Analysis of Future Automotive Fuels and Powertrains in the European Context," *SAE Technical Paper* 2004-01-1924.
2. Rousseau, A., Wallner, T., Pagerit, S., and Lohse-Busch, H., 2008, "Prospects on Fuel Economy Improvements for Hydrogen-Powered Vehicles," *SAE Technical Paper* 2008-01-2378.

3. Delorme, A., Rousseau, A., Sharer, P., Pagerit, S., and Wallner, T., 2009, "Evolution of Hydrogen Fueled Vehicles Compared to Conventional Vehicles from 2010 to 2045," *SAE Technical Paper* 2009-01-1008.
4. White, C. M., Steeper, R. R., and Lutz, A. E., 2006, "The Hydrogen-Fueled Internal Combustion Engine: A Technical Review," *Int. J. Hydrogen Energy* 31(10):1292-1305.
5. Mohammadi, A., Shioji, M., Nakai, Y., Ishikura, W., and Tabo, E., 2007, "Performance and Combustion Characteristics of a Direct Injection SI Hydrogen Engine," *Int. J. Hydrogen Energy* 32(2):296-304.
6. Salazar, V. M. and Kaiser, S. A., 2009, "An Optical Study of Mixture Preparation in a Hydrogen-Fueled Engine with Direct Injection Using Different Nozzle Designs," *SAE Technical Paper* 2009-01-2682.
7. Wallner, T., Nande, A. M., and Naber, J. D., 2009, "Study of Basic Injection Configurations using a Direct-Injection Hydrogen Research Engine," *SAE Technical Paper* 2009-01-1008.
8. Verhelst, S. and Wallner, T., 2009, "Hydrogen-Fueled Internal Combustion Engines," *Prog. Energy Combust. Sci.* 35:490-527.
9. Heywood, J. B., "Internal Combustion Engine Fundamentals", McGrawHill, New York, 1988.
10. Aleiferis, P. G., Taylor, A. M. K. P., Whitelaw, J. H., Ishii, K., and Urata, Y., 2000, "Cyclic Variations of Initial Flame Kernel Growth in a Honda VTEC-E Lean-Burn Spark-Ignition Engine," *SAE Technical Paper* 2000-01-1207.
11. Aleiferis, P. G., Taylor, A. M. K. P., Ishii, K., and Urata, Y., 2004, "The Relative Effects of Fuel Concentration, Residual-Gas Fraction, Gas Motion, Spark Energy and Heat Losses to the Electrodes on Flame-Kernel Development in a Lean-Burn Spark Ignition Engine," *Proc. Inst. Mech. Eng. Part D-J. Automob. Eng.* 218:411-425.
12. Hicks, R. A., Lawes, M., Sheppard, C. G. W., and Whitaker, B. J., 1994, "Multiple Laser Sheet Imaging Investigation of Turbulent Flame Structure in a Spark Ignition Engine," *SAE Technical Paper* 941992.
13. Mouqallid, M., Lecordier, B., and Trinite, M., 1994, "High Speed Laser Tomography Analysis of Flame Propagation in a Simulated Internal Combustion Engine - Applications to Nonuniform Mixture," *SAE Technical Paper* 941990.
14. Arcoumanis, C., Godwin, S. N., and Kim, J. W., 1998, "Effect of Tumble Strength on Combustion and Exhaust Emissions in a Single-Cylinder, Four-Valve, Spark-Ignition Engine," *SAE Technical Paper* 981044.
15. Cairns, J. and Sheppard, C. G. W., 2000, "Cyclically Resolved Simultaneous Flame and Flow Imaging in a SI Engine," *SAE Technical Paper* 2000-01-2832.
16. Kuwahara, K. and Ando, H., 2000, "Diagnostics of In-Cylinder Flow, Mixing and Combustion in Gasoline Engines," *Meas. Sci. Technol.* 11:95-111.
17. Pajot, O. and Mounaim-Rousselle, C., 2000, "Instantaneous Flow Field Effects on the Flame Kernel in S.I. Engines by Simultaneous Optical Diagnostics," *SAE Technical Paper* 2000-01-1796.
18. Oh, S., Kim, S., Bae, C., Kim, C., and Kang, K., 2002, "Flame Propagation Characteristics in a Heavy Duty LPG Engine with Liquid Phase Port Injection," *SAE Technical Paper* 2002-01-1736.
19. Hacohen, J., Belmont, M. R., and Ashcroft, S. J., 1994, "Flame Speeds in a Spark Ignition Engine," *SAE Technical Paper* 942050.
20. Aleiferis, P. G., Hardalupas, Y., Taylor, A. M. K. P., Ishii, K., and Urata, Y., 2004, "Flame Chemiluminiscence Studies of Cyclic Combustion Variations and Air-to-Fuel Ratio of the Reacting Mixture in a Lean-Burn Stratified-Charge Spark-Ignition Engine," *Combust. Flame* 136:72-90.
21. Lumley, J. L., "Engines: An Introduction", Cambridge University Press, New York, 1999.
22. Lancaster, D. R., Krieger, R. B., Sorenson, S. C., and Hull, W. L., 1976, "Effects of Turbulence on Spark-Ignition Engine Combustion," *SAE Technical Paper* 760160.
23. Ozdor, N., Dulger, M., and Sher, E., 2000, "Cyclic Variability in a Spark-Ignition Engine - A Literature Survey," *SAE Technical Paper* 940987.
24. Aleiferis, P. G., Taylor, A. M. K. P., Ishii, K., and Urata, Y., 2004, "The Nature of Early Flame Development in a Lean-Burn Stratified-Charge Spark-Ignition Engine," *Combust. Flame* 136:283-302.
25. Bates, S., 1989, "Flame Imaging Studies of Cycle to Cycle Combustion Variation in a SI Four Stroke Engine," *SAE Technical Paper* 892083.
26. Bates, S. C., 1989, "Flame Imaging Studies in a Spark-Ignition Four-Stroke Internal Combustion Optical Engine," *SAE Technical Paper* 890154.
27. Bates, S., 1991, "Further Insights into SI Four-Stroke Combustion Using Flame Imaging," *Combust. Flame* 85:331-352.
28. Hill, P. G. and Zhang, D., 1994, "The Effects of Swirl and Tumble on Combustion in Spark-Ignition Engines," *Prog. Energy Combust. Sci.* 20(5):373-429.
29. Boree, J., Maurel, S., and Bazile, R., 2002, "Disruption of a Compressed Vortex," *Phys. Fluids* 14(7):2543-2556, doi:10.1063/1.1472505.
30. Moreau, J., Boree, J., Bazile, R., and Charnay, G., 2004, "Destabilisation of a Compressed Vortex by a Round Jet," *Exp. Fluids* 37(6):856-871, doi:10.1007/s00348-004-0869-0.
31. Salazar, V. M. and Kaiser, S. A., 2010, "Influence of the In-Cylinder Flow Field (Tumble) on the Fuel Distribution in a DI Hydrogen Engine Using a Single-Hole Injector," *SAE Technical Paper* 2010-01-0579.

32. Salazar, V. M. and Kaiser, S. A., 2010, "Characterization of Mixture Preparation in a Direct-Injection Internal Combustion Engine Fueled with Hydrogen usign PIV and PLIF," *15th Int. Symp. on Applications of Laser Techniques to Fluid Mechanics, Lisbon Portugal, 05-08 July, 2010* Paper 1773.
33. Salazar, V. M. and Kaiser, S. A., 2011, "Interaction of Intake-Induced Flow and Injection Jet in a Direct-Injection Hydrogen-Fueled Engine Measure by PIV," *SAE Technical Paper* 2011-01-0673.
34. Milton, B. E. and Keck, J. C., 1984, "Laminar Burning Velocities in Stoichiometric Hydrogen and Hydrogen-Hydrocarbon Gas Mixtures," *Combust. Flame* 58:13-22.
35. Verhelst, S., Woolley, R., Lawes, M., and Sierens, R., 2005, "Laminar and Unstable Burning Velocities and Markstein Lengths of Hydrogen-Air Mixtures at Engine Like Conditions," *Proc. Combust. Inst.* 30:209-216.
36. Bradley, D., Lawes, M., Liu, K., Verhelst, S., and Woolley, R., 2007, "Laminar Burning Velocities of Lean Hydrogen-Air Mixtures at Pressures up to 1.0 MPa," *Combust. Flame* 149:162-172.
37. Picket, L. M., *Vol. 2010,*2010.
38. G.S.Settles, "Schlieren and Shadowgraph Techniques", Springer, Berlin, 2001.
39. Pickett, L. M., Kook, S., and Williams, T. C., 2009, "Visualization of Diesel Spray Penetration, Cool-Flame, Ignition, High-Temperature Combustion, and Soot Formation Using High-Speed Imaging," *SAE Technical Paper* 2009-01-0658.
40. McMillian, M., Richardson, S., Woodruff, S. D., and McIntyre, D., 2004, "Laser-Spark Ignition Testing in a Natural Gas-Fueled Single-Cylinder Engine," *SAE Technical Paper* 2004-01-0980.
41. Alger, T., Mehta, D., Chadwell, C., and Roberts, C., 2005, "Laser Ignition in a Pre-Mixed Engine: The Effect of Focal Volume and Energy Density on Stability and the Lean Operating Limit," *SAE Technical Paper* 2005-01-3752.
42. Mullett, J. D., Dickinson, P. B., Shenton, A. T., Dearden, G., and Watkins, K. G., 2008, "Multi-Cylinder Laser and Spark Ignition in an IC Gasoline Automotive Engine: A Comparative Study," *SAE Technical Paper* 2008-01-0470.
43. Srivastava, D. K., Weinrotter, M., Iskrac, K., Agarwal, A. K., and Wintner, E., 2009, "Characterisation of laser ignition in hydrogen–air mixtures in a combustion bomb," *Int. J. Hydrogen Energy* 34:2475-2482, doi:10.1016/j.ijhydene.2008.11.117.
44. He, Y., Selamet, A., Reese, R. A., Vick, R. K., and Amer, A. A., 2007, "Impact of Tumble on Combustion in SI Engines: Correlation Between Flow and Engine Experiments," *SAE Technical Paper* 2007-01-4003.
45. Fajardo, C. M., Smith, J. D., and Sick, V., 2006, "PIV, High-Speed PLIF and Chemiluminescence Imaging for near-Spark-Plug Investigations in IC Engines," *Journal of Physics: Conference Series, ICOLAD 2005* 45:19-26.
46. Muller, S. H. R., Bohm, B., Gleissner, M., and Arndt, S., 2010, "Analysis of the Temporal Flame Kernel Development in an Optically Accessible IC Engine Using High-Speed OH-PLIF," *Appl. Phys. B - Lasers Opt.* 100:447-452.
47. Salazar, V. M. and Ghandhi, J., 2008, " Ring Pack Crevices and Crankcase Pressure Effects on the Hydrocarbon Emissions from an Air-Cooled Utility Engine," *SAE Technical Paper* 2008-32-0004.

CONTACT INFORMATION

Victor Salazar vmsalaz@sandia.gov

Sebastian Kaiser sebastian.kaiser@uni-due.de